

# Inversion of Sea Surface Chlorophyll Concentration from Coastal Zone Imager Onboard China's Ocean Color Satellite HY-1C

Shaojun Gong,<sup>1</sup> Chao Chen,<sup>2,3\*</sup> Xingbai Hu,<sup>4</sup> and Taohua Ren<sup>4</sup>

<sup>1</sup>Marine Science and Technology College, Zhejiang Ocean University, Zhoushan 316022, China

<sup>2</sup>School of Geography Science and Geomatics Engineering, Suzhou University of Science and Technology, Suzhou 215009, China

<sup>3</sup>State Key Laboratory of Remote Sensing Science, Aerospace Information Research Institute, Chinese Academy of Sciences, Beijing 100101, China

<sup>4</sup>School of Information Engineering, Zhejiang Ocean University, Zhoushan 316022, China

(Received August 9, 2024; accepted January 15, 2025)

**Keywords:** coastal waters, sea surface chlorophyll concentration, HY-1C, CZI, remote sensing inversion

Sea surface chlorophyll concentration is one of the critical parameters of ocean color. It serves as a fundamental indicator for assessing marine net primary productivity and eutrophication. However, obtaining accurate data and conducting rapid sea surface chlorophyll concentration measurements present significant challenges. This study is based on the Coastal Zone Imager (CZI) data from China's ocean color satellite HY-1C, which analyzes the sensitivity of spectral bands, and a remote sensing inversion model for sea surface chlorophyll concentration, which is suitable for the coastal waters of China, was constructed. The experimental results in the coastal waters near the Zhoushan Archipelago indicate the following: (1) The band combinations  $B3/B2$  and  $B3/(B2 + B1)$  exhibit the highest correlation with sea surface chlorophyll concentration, with a correlation coefficient of 0.77. (2) The quadratic polynomial model ( $y = 105.42x^2 - 175.67x + 75.167$ ) constructed using  $B3/B2$  as the independent variable demonstrates the highest inversion accuracy for sea surface chlorophyll concentration. The  $R^2$  value is 0.9107 and the mean absolute percentage error is 26.85%. This study plays a significant role in advancing the operational level of domestic ocean satellites and in monitoring coastal water quality.

## 1. Introduction

Sea surface chlorophyll concentration is one of the important indicators for measuring the health of the marine ecological environment.<sup>(1,2)</sup> It can not only reflect the abundance and developmental status of phytoplankton in the seawater, but it is also related to the productivity of the marine ecosystem, biodiversity, and the sustainable utilization of fishery resources.<sup>(3–5)</sup>

Currently, there are two main methods for obtaining sea surface chlorophyll concentration: direct measurement and remote-sensing-based methods.<sup>(6)</sup> The direct measurement method involves field sampling. In the laboratory, fluorescence spectrophotometry is used to isolate sea

---

\*Corresponding author: e-mail: [chenchao@usts.edu.cn](mailto:chenchao@usts.edu.cn)  
<https://doi.org/10.18494/SAM5288>

surface chlorophyll from these samples, and the concentration of sea surface chlorophyll is then calculated on the basis of results.<sup>(7,8)</sup> The remote-sensing-based method uses the law of variation of the spectral curve of a water body with the different substances contained in the seawater, identifying the correlation between reflectance spectra in different bands and sea surface chlorophyll concentration, thereby constructing a remote sensing inversion model for sea surface chlorophyll concentration.<sup>(9,10)</sup> The direct measurement method provides high precision, is time-consuming and labor-intensive, and has high economic costs. Additionally, owing to the complex nearshore geographical environment, strong ocean currents, and the impact of operators and sampling methods, the direct measurement method has limitations in reflecting the nearshore marine environment in terms of sea surface chlorophyll concentration. The remote-sensing-based method can overcome these limitations, allowing for the real-time monitoring of sea surface chlorophyll concentration. It not only reflects the spatial and temporal changes in the marine environment but also reveals pollution sources and pollutant migration characteristics that are difficult to detect by conventional methods. This method has the advantages of being unrestricted by geographical areas, fast, cost-effective, and capable of long-term dynamic monitoring.<sup>(11–13)</sup>

The Coastal Zone Imager (CZI) is a sensor onboard China's ocean color satellite HY-1C. It offers benefits such as a short revisit cycle (3 days) and a high signal-to-noise ratio, making it widely used in algal bloom monitoring and other related fields.<sup>(14)</sup> In this study, which is tailored to the characteristics of HY-1C CZI data, we utilized field-measured spectral data and sea surface chlorophyll concentration data to analyze the sensitive bands for the remote sensing inversion of sea surface chlorophyll concentration. We constructed a remote sensing inversion model for sea surface chlorophyll concentration in coastal waters for the monitoring of marine environments.

## 2. Study Area and Data Sources

### 2.1 Study area

The Zhoushan Archipelago (121°30'–123°25'E, 29°32'–31°04'N) is under the jurisdiction of Zhejiang Province and comprises 2085 islands, accounting for approximately 20% of the total number of islands in China.<sup>(15,16)</sup> For the Zhoushan Archipelago with its numerous islands and abundant fishery resources, data from domestic ocean satellites are utilized to study the ecological elements of the coastal waters surrounding it.<sup>(17,18)</sup> The location of the study area is shown in Fig. 1.

### 2.2 Data sources

The data utilized in this study comprise HY-1C CZI data, field-measured spectral data, and sea surface chlorophyll concentration data.

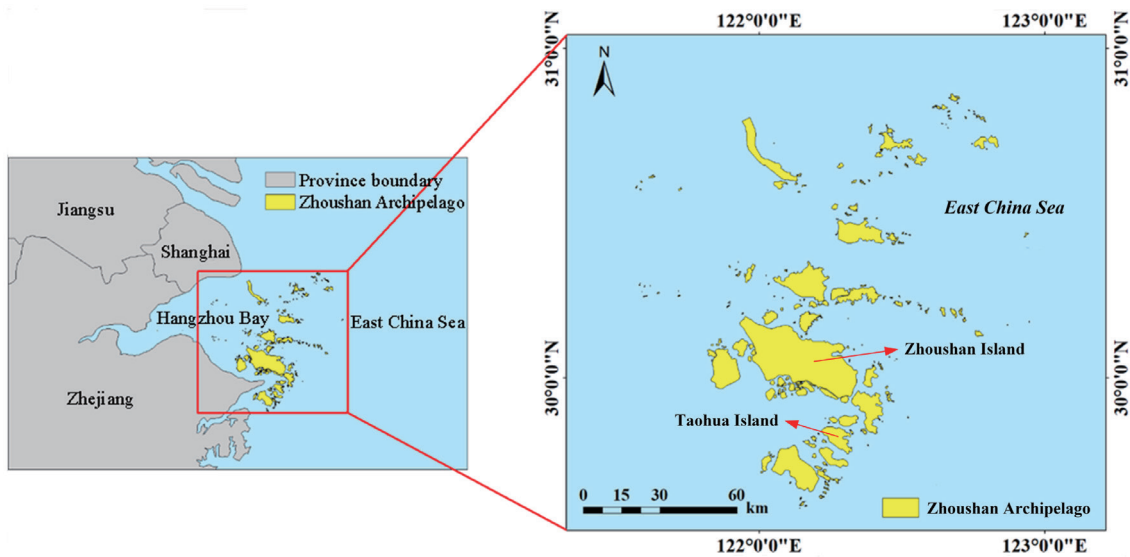


Fig. 1. (Color online) Location of study area.

### 2.2.1 HY-1C CZI data

In September 2018, China launched the ocean color satellite HY-1C, which is equipped with five sensors: the Chinese Ocean Color and Temperature Scanner, CZI, the Ultra-Violet Imager (UVI), the Satellite-based Calibration Spectrometer (SCS), and the Automatic Identification System (AIS).<sup>(19–23)</sup> Among them, the CZI has four bands, namely, red, green, blue, and near-infrared, with a spatial resolution higher than 50 m and an observation swath width greater than 950 km; it is mainly used for observing coastal waters, islands, and coastal zones. The main parameters of the HY-1C CZI are shown in Table 1.<sup>(24)</sup> After specific processing, the CZI data product in specific levels can be obtained. In this study, the remote sensing reflectance of CZI data was used, and radiometric calibration and atmospheric correction were performed. The pixel gray value was converted to radiance by physical means using calibration parameters through radiometric calibration, and atmospheric correction was performed to reduce the effects of atmospheric scattering and absorption on radiance and obtain reflectance data.

### 2.2.2 Field-measured data

From September 24–26, 2021 and March 7–9, 2022, two field spectral data sampling tasks were conducted on Taohua Island in Zhoushan, resulting in 25 sets of field spectral data and sea surface chlorophyll concentration data. The distribution of the sampling points is shown in Fig. 2.

#### 2.2.2.1 Measured spectral data of water body

The sampling process utilized China's first amphibious field spectrometer, the ISI921VF-512 (shown in Table 2). To minimize the impact of water body surface specular reflection and boat

Table 1  
Parameter setting and main application of satellite HY-1C.

Band number	Spectral range (nm)	Resolution	Revisit cycle	Satellite altitude	Application
1	0.42–0.50	50 m	3 days	782 km	Chlorophyll, Pollution, Ice, Shallow marine terrain
2	0.52–0.60				Chlorophyll, Low-concentration sediment, Pollution, Tidal flat
3	0.61–0.69				Moderate sediment, Vegetation, Soil
4	0.76–0.89				vegetation, High-concentration sediment, Atmospheric correction

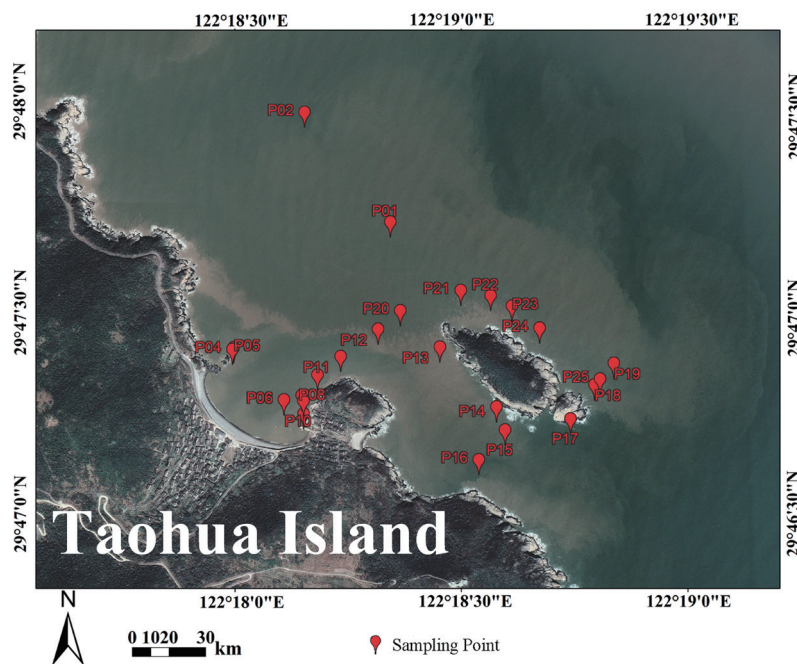


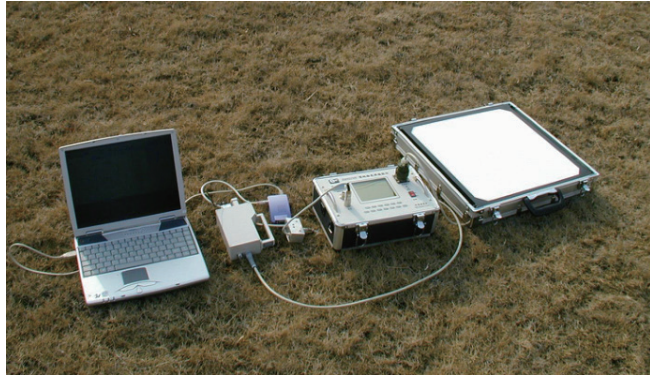
Fig. 2. (Color online) Location of sampling points.

shadow on the measurement results, and to better extract the water-leaving radiance and remote sensing reflectance that reflect the water body information, a certain observation angle is adopted for water body spectral observation during the measurement. The angle between the instrument's observation plane and the sun's incidence plane is 90 to 135° (against the direction of the sun), and the angle between the instrument and the water surface normal is about 30 to 45°. Simultaneously, the skylight has a reflection on the surface, and this reflected component must be excluded to obtain unitary water body information. Therefore, after the instrument is oriented toward the water body for measurement, the instrument must be rotated upward by a specific angle within the observation plane (usually 90°, so that the zenith angle for the skylight observation is the same as the observation angle during the water surface measurement) to measure the radiance information of the skylight.

The spectral curve of a water body is the most direct manifestation of its optical characteristic and is the most widely used optical statistical information in ocean color research. It can

Table 2

(Color online) Parameters of the ground-object spectroradiometer ISI921VF-512.

Ground-object spectroradiometer ISI921VF-512	
	
Spectral range	380–1050 nm (The spectral range can be adjusted by $\pm 30$ nm on the basis of user requirements.)
Spectral resolution	2 nm (512 channels)
Wavelength accuracy	0.7 nm
Signal-to-noise ratio	Equivalent noise radiance $1 \times 10^{-9} \text{W} \cdot \text{cm}^{-2} \cdot \text{nm}^{-1} \cdot \text{sr}^{-1}$
Measurement accuracy	2%
Continuous runtime	5 h
Sensor head	1.0 kg $174 \times 115 \times 51 \text{mm}$
Main device	3.8 kg $285 \times 198 \times 100 \text{mm}$
Number of stored curves	512 curves
Two-meter measurement rod	present
Laser indicator	present
Additional functions	GPS, video recording, and other functions

intuitively reflect the law of variation in the radiation energy of the water body affected by absorption and scattering, and analyzing the spectral characteristics of a water body can provide insights into the composition of the water and the impact of each component on the spectral curve.<sup>(25,26)</sup> Equation (1) is used to convert the data obtained from the spectrometer into remote sensing reflectance (shown in Fig. 3).

$$R_{rs} = \frac{(I_{wat} - \alpha \cdot I_{sky}) \cdot R_p}{\pi \cdot I_p} \quad (1)$$

Here,  $R_{rs}$  is the remote sensing reflectance of the water body,  $I_{wat}$  is the radiance measured by the spectrometer,  $\alpha$  is the water surface reflectance, which is taken as 0.028 in the calculation,  $I_{sky}$  is the radiance from the sky's diffuse reflection,  $I_p$  is the radiance from the reference panel, and  $R_p$  is the reflectance of the reference panel.

The remote sensing reflectance of the water body derived from 25 sets of field-measured spectral data is shown in Fig. 3. In the wavelength range of 380–500 nm, the curve has a small slope, the increase is relatively slow, and the overall trend is smooth, as shown in Fig. 3. This is due to the absorption effects of sea surface chlorophyll and other soluble organic materials. After 500 nm, the growth of the water body's spectral curve begins to accelerate, reaching a peak

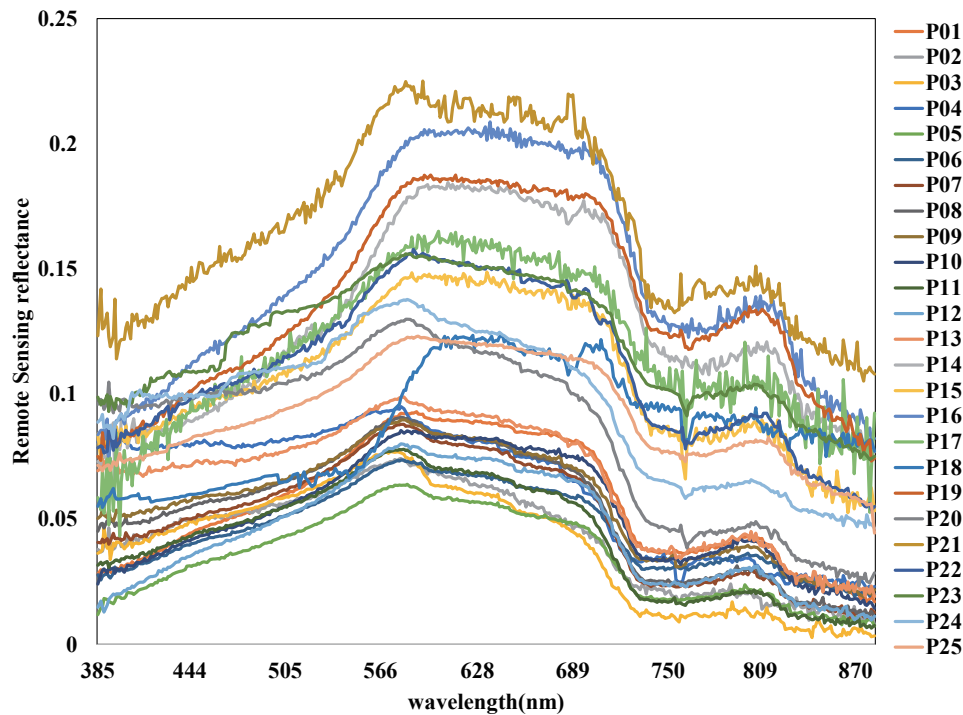


Fig. 3. (Color online) Spectral curves of water with different sea surface chlorophyll concentrations in the coastal waters of Zhoushan. The horizontal axis is wavelength, the vertical axis is remote sensing reflectance, and the curve reflects the change in remote sensing reflectance with wavelength.

around 577 nm. In the wavelength range of 577–700 nm, the reflectance values fluctuate minimally, forming a “broad peak” phenomenon. Some sampling points exhibit a minor reflection at 640 nm, primarily due to the absorption effect of sea surface chlorophyll in this wavelength interval. Different concentrations of chlorophyll have varying impacts on the spectral curve. Around 710 nm, there are sudden increases in values, which are attributed to the increase caused by the reflection of chlorophyll. In the wavelength range of 770–810 nm, the values initially rise and then fall, with a lower peak, which is approximately half of the maximum peak value, and a smaller width. This phenomenon is caused by the scattering of surface-suspended particles. After 870 nm, the effects of environmental factors lead to a high level of noise, significantly reducing the validity of the data; therefore, they were excluded.

#### 2.2.2.2 Measured sea surface chlorophyll concentration data

In this study, the domestically produced YG-multi-parameter water quality sensor was utilized to measure the sea surface chlorophyll concentration at a depth of 50 cm by the fluorescence method. The technical parameters of the YG-multi-parameter water quality sensor are shown in Table 3. The sea surface chlorophyll concentrations at the various sampling points are shown in Table 4.

Table 3  
(Color online) Technical parameters of YG-multi-parameter water quality sensor.


YG -multi-parameter water quality sensor	
	
Measurement range	0–400 µg/L or 0–100 RFU
Accuracy	±5% or 0.5 µg/L, whichever is greater
Resolution	0.01 µg/L
Protection rating	IP68
Temperature range	0–50 °C
Sensor interface	Supports RS-485, MODBUS protocol
Power information	DC 12–24 V

Table 4  
Sea surface chlorophyll concentrations at various sampling points.

Sampling point	Longitude and latitude	Sea surface chlorophyll concentration (µg/L)	Sampling point	Longitude and latitude	Sea surface chlorophyll concentration (µg/L)
P01	(122.31686 E, 29.79153 N)	5.2703	P14	(122.32012 E, 29.78399 N)	11.691
P02	(122.31116 E, 29.78751 N)	1.6041	P15	(122.32339 E, 29.78532 N)	7.5979
P03	(122.31120 E, 29.78756 N)	1.406	P16	(122.32423 E, 29.78639 N)	13.998
P04	(122.31304 E, 29.78593 N)	2.0626	P17	(122.32511 E, 29.78715 N)	9.091
P05	(122.31368 E, 29.78606 N)	2.0789	P18	(122.31721 E, 29.78877 N)	2.8347
P06	(122.31424 E, 29.78671 N)	3.3407	P19	(122.31939 E, 29.78938 N)	11.5649
P07	(122.31376 E, 29.78550 N)	2.7913	P20	(122.32049 E, 29.78919 N)	2.8468
P08	(122.31374 E, 29.78589 N)	2.7018	P21	(122.32128 E, 29.78886 N)	3.9012
P09	(122.31508 E, 29.78729 N)	2.7329	P22	(122.32232 E, 29.78811 N)	6.8351
P10	(122.31642 E, 29.78814 N)	3.9927	P23	(122.32446 E, 29.78658 N)	8.4579
P11	(122.31866 E, 29.78760 N)	4.632	P24	(122.32538 E, 29.78689 N)	7.3662
P12	(122.32070 E, 29.78571 N)	5.5864	P25	(122.31839 E, 29.79051 N)	5.4649
P13	(122.32101 E, 29.78499 N)	3.9073			

### 3. Methods

This study is based on the CZI remote sensing data from China's ocean color satellite HY-1C. We used the remote sensing inversion method to determine the sea surface chlorophyll concentration, with the specific process shown in Fig. 4. This study encompasses four components: image preprocessing, band sensitivity analysis, model establishment, and accuracy assessment.

#### 3.1 Image preprocessing

Radiometric calibration and reflectance correction were performed on the HY-1C CZI data to obtain reflectance data.

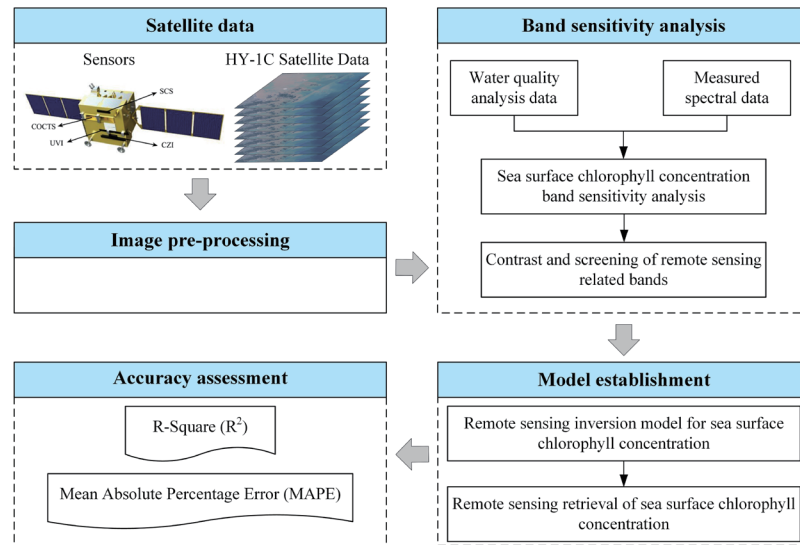


Fig. 4. (Color online) Technical flowchart.

### 3.2 Band sensitivity analysis

In the remote sensing inversion of key ocean color parameters in coastal waters, the spectral curve of the water body is a result of the combined effects of water molecules, sea surface chlorophyll, suspended sediments, and other ocean color elements. Therefore, to construct a more accurate remote sensing inversion model for sea surface chlorophyll concentration, we comprehensively considered single bands, different band combinations, and remote sensing indices (such as *NDWI*, *NDVI*, and *EVI*) to deeply explore the relationship between satellite remote sensing data and sea surface chlorophyll concentration. We statistically analyzed the correlation coefficients between single bands, different band combinations, and remote sensing indices with the field-measured chlorophyll concentrations, selecting the spectral band with the highest correlation coefficient as the sensitive band. The sensitivity analysis of sea surface chlorophyll concentration is shown in Table 5.

From Table 5, in terms of single bands, the correlation coefficients of the HY-1C CZI data's *B1*, *B2*, *B3*, and *B4* with sea surface chlorophyll concentration are  $-0.23$ ,  $0.14$ ,  $0.55$ , and  $0.48$ , respectively, with *B3* (red band) showing the highest correlation. In terms of different band combinations, the correlation coefficient of  $B3/B2$  and  $B3/(B1 + B2)$  with sea surface chlorophyll concentration is  $0.77$ . In terms of remote sensing indices, the correlation coefficients of *NDWI*, *NDVI*, and *EVI* with sea surface chlorophyll concentration are  $-0.43$ ,  $0.27$ , and  $-0.45$ , respectively. Therefore, in this study, we selected  $B3/B2$  and  $B3/(B1 + B2)$  as the sensitive factors for the remote sensing inversion of sea surface chlorophyll concentration.

### 3.3 Construction of RS inversion model of sea surface chlorophyll concentration

On the basis of the band sensitivity analysis of sea surface chlorophyll concentration, the band combinations  $B3/B2$  and  $B3/(B1 + B2)$  were selected as independent variables. Models were



Table 5

Analysis table of correlation between measured spectral data and chlorophyll concentration at sea surface.

Independent variable	Correlation coefficient	Independent variable	Correlation coefficient	Independent variable	Correlation coefficient	Independent variable	Correlation coefficient
$B1$	-0.23	$B2/B1$	0.61	$B4/(B3 + B2)$	0.35	$NDWI$	-0.43
$B2$	0.14	$B3/B1$	0.74	$B4/(B1 + B2)$	0.51	$NDVI$	0.27
$B3$	0.55	$B4/B1$	0.60	$B3/(B1 + B2)$	0.77	$EVI$	-0.45
$B4$	0.48	$B3/B2$	0.77	$(B4 + B3)/B2$	0.63		
		$B4/B2$	0.42	$(B2 + B3)/B1$	0.69		
		$B4/B3$	0.26	$(B3 + B4)/(B2 + B1)$	0.72		
				$B4/(B3 + B2 + B1)$	0.44		

Note: In the table,  $B1$ ,  $B2$ ,  $B3$ , and  $B4$  respectively represent the blue, green, red, and near-infrared bands of the CZI remote sensing data from the satellite HY-1C.

constructed in mathematical forms such as linear, quadratic polynomial, exponential, and logarithmic to reverse the sea surface chlorophyll concentration in the Zhoushan coastal waters, with the precision of the models assessed using the  $R^2$ .

$R^2$  is commonly used to represent the fit between two sets of data; the larger the  $R^2$ , the better the model fits the data.

$$R^2 = \frac{\sum_{i=1}^n (y_i - \bar{y})^2 - \sum_{i=1}^n (y_i - f_i)^2}{\sum_{i=1}^n (y_i - \bar{y})^2} \quad (2)$$

Here,  $n$  is the number of observations,  $y_i$  is the true observed value of the  $i$ -th instance,  $f_i$  is the predicted value for the  $i$ -th observation, and  $\bar{y}$  is the mean of all true observed values. The sea surface chlorophyll concentration remote sensing reversion model constructed in this study and its accuracy assessment results are shown in Table 6.

From Table 6, with the band combination  $B3/B2$  as the independent variable, the reversion model constructed in the form of a quadratic polynomial has the highest  $R^2$ , which is 0.9107, indicating that this model has the highest precision. Therefore, this model is selected as the remote sensing reversion model for sea surface chlorophyll concentration using HY-1C CZI data, and its formula is as follows:

$$y = 105.42x^2 - 175.67x + 75.167, \quad (3)$$

where  $x$  is the ratio of remote sensing reflectance between the red and green bands of the HY-1C CZI data.

### 3.4 Accuracy assessment

Accuracy assessment is an essential step in remote sensing information extraction and target identification, serving as an important basis for assessing model accuracy and adjusting model

Table 6  
Remote sensing inversion model construction with sea surface chlorophyll concentration.

Independent variable	Model	Formula	$R^2$
$B3/B2$	linear	$y = 37.04x - 31.207$	0.8393
	quadratic polynomial	$y = 105.42x^2 - 175.67x + 75.167$	0.9107
	exponential	$y = 0.0069e^{6.5394x}$	0.9034
	logarithmic	$y = 36.708\ln(x) + 5.9961$	0.8397
$B3/(B1 + B2)$	linear	$y = 45.446x - 20.831$	0.7848
	quadratic polynomial	$y = 163.17x^2 - 146.25x + 34.603$	0.8563
	exponential	$y = 0.0416e^{8.0926x}$	0.8640
	logarithmic	$y = 25.767\ln(x) + 19.786$	0.7513

Note:  $y$  represents the sea surface chlorophyll concentration;  $x$  represents the remote sensing reflectance ratios of  $B3/B2$  and  $B3/(B1 + B2)$ .

parameters.<sup>(27,28)</sup> Table 6 indicates that there are four models with an  $R^2$  greater than 0.85. These include the quadratic polynomial model and the exponential model with  $B3/B2$  as the independent variable, with  $R^2$  values of 0.9107 and 0.9034, and the quadratic polynomial model and the exponential model with  $B3/(B1 + B2)$  as the independent variable, with  $R^2$  values of 0.8563 and 0.864, respectively. In this study, 10 out of 25 sampling points were selected to conduct an accuracy verification of the inversion results.

The mean absolute percentage error ( $MAPE$ ) is a parameter for assessing accuracy, with a smaller value indicating a more precise model.<sup>(29,30)</sup>

$$MAPE(\%) = \frac{1}{n} \cdot \sum_{i=1}^n \left| \frac{(y_i - f_i)}{y_i} \right| \cdot 100\% \quad (4)$$

Here,  $n$  is the number of observations,  $y_i$  is the actual value at the  $i$ -th instance, and  $f_i$  is the predicted value at the  $i$ -th instance.

The comparison results between the field-measured sea surface chlorophyll concentration and the chlorophyll concentration calculated using the model are presented in Table 7. For the model with  $B3/B2$  as the independent variable, the quadratic polynomial model yielded a maximum error of 49.50% and a minimum error of 12.63%, with a  $MAPE$  of 26.85%. The exponential model resulted in a maximum error of 63.92% and a minimum error of 16.55%, with a  $MAPE$  of 32.03%. For the model with  $B3/(B1 + B2)$  as the independent variable, the quadratic polynomial model showed a maximum error of 73.77% and a minimum error of 6.49%, with a  $MAPE$  of 35.04%. The exponential model had a maximum error of 70.28% and a minimum error of 19.71%, with a  $MAPE$  of 38.20%.

#### 4. Results and Analysis

We used Rayleigh-scattering-corrected HY-1C CZI L2A remote sensing reflectance data for the reversion of sea surface chlorophyll concentration. The remote sensing data comes from the National Satellite Ocean Application Service Center of China (<https://osdds.nsoas.org.cn>). A total of seven scenes of imagery were used, covering the Zhoushan Archipelago and its coastal

Table 7

Summary of accuracy of sea surface chlorophyll concentration inversion model in Zhoushan coastal waters.

Independent variable	Reversion model	Mathematical formula	$R^2$	MAPE
$B3/B2$	quadratic polynomial	$y = 105.42x^2 - 175.67x + 75.167$	0.9107	26.85%
	exponential	$y = 0.0069e^{6.5394x}$	0.9034	32.03%
$B3/(B1 + B2)$	quadratic polynomial	$y = 163.17x^2 - 146.25x + 34.603$	0.8563	35.04%
	exponential	$y = 0.0416e^{8.0926x}$	0.864	38.20%

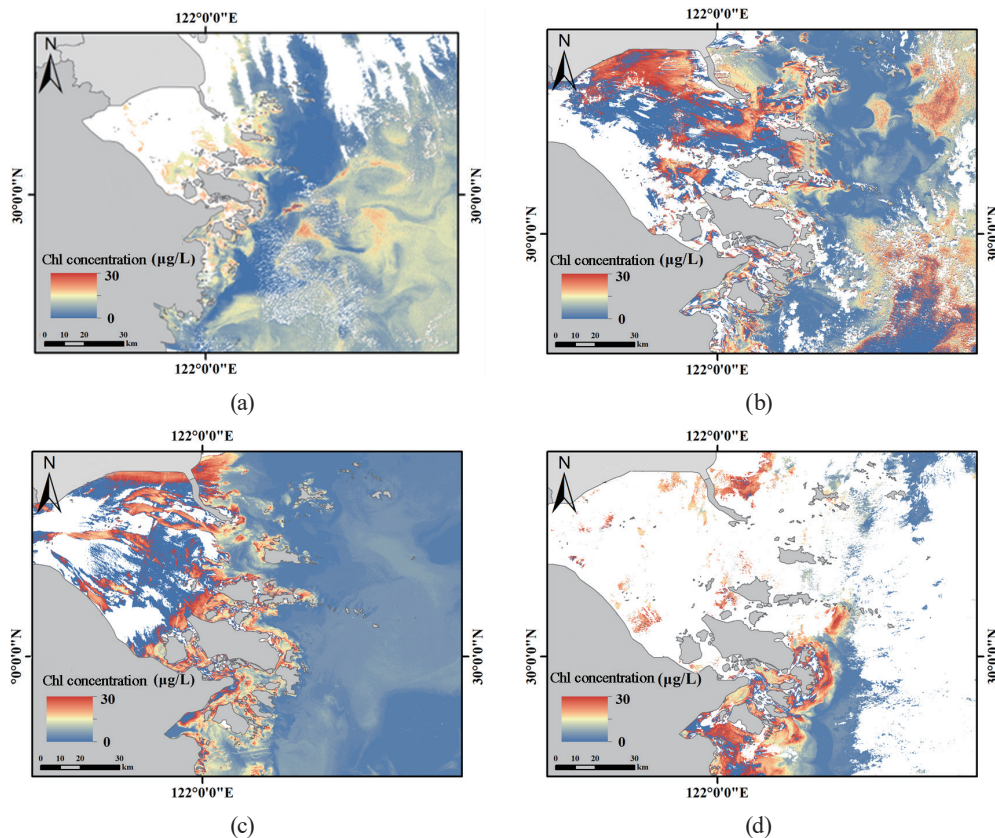


Fig. 5. (Color online) Inversion results of sea surface chlorophyll concentration in Zhoushan coastal waters. (a) 2021.09.25, (b) 2021.10.10, (c) 2021.11.15, (d) 2021.12.09, (e) 2022.01.11, (f) 2022.02.25, and (g) 2022.03.09.

waters. The imaging dates are September 25, 2021, October 10, 2021, November 15, 2021, December 9, 2021, January 11, 2022, February 25, 2022, and March 9, 2022.

Utilizing the sea surface chlorophyll concentration remote sensing reversion model [Eq. (3)] constructed in this study and on the basis of HY-1C CZI remote sensing data, we obtained the sea surface chlorophyll concentration of the Zhoushan Archipelago coastal waters (Fig. 5). Figure 5 shows that the inversion results accurately reflect the spatiotemporal distribution of sea surface chlorophyll concentration in the coastal waters near the Zhoushan Archipelago, where the coastal waters have higher concentrations, exceeding  $20 \mu\text{g/L}$ , and the values in seas farther from land were generally lower than  $10 \mu\text{g/L}$ .

By comparing the two sets of inversion results from September and October, we observed that there are areas with low chlorophyll concentrations in the nearshore regions, with distinct

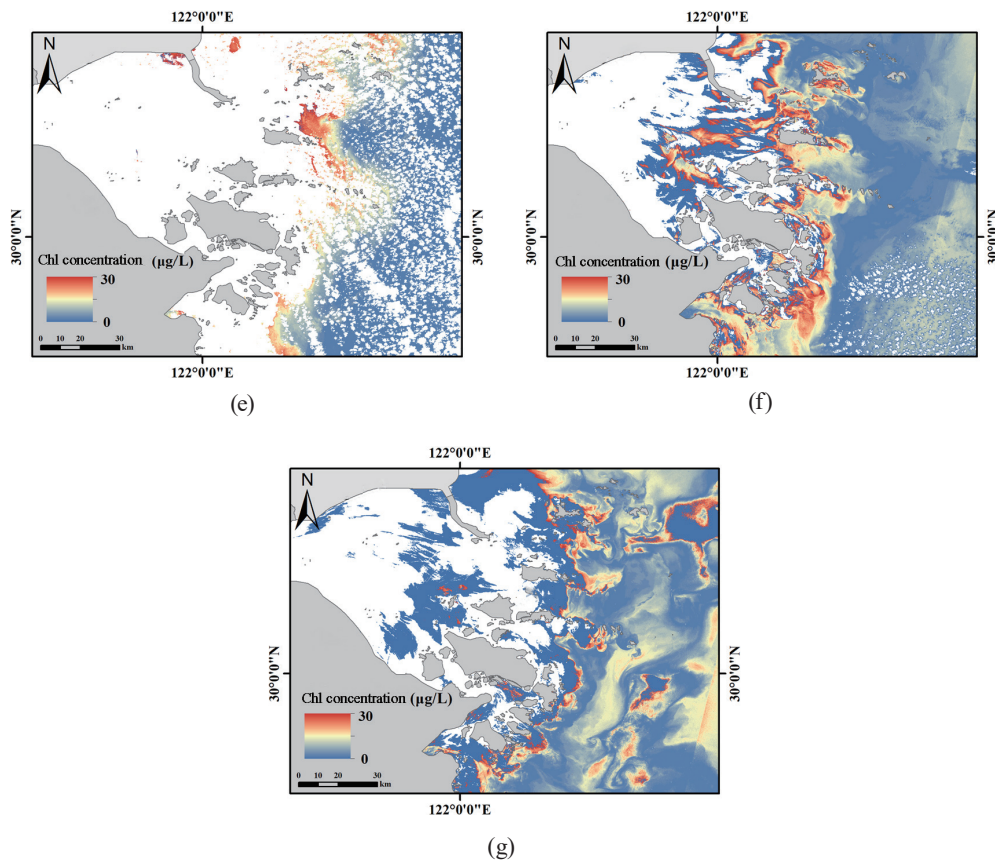


Fig. 5. (Color online) (Continued) Inversion results of sea surface chlorophyll concentration in Zhoushan coastal waters. (a) 2021.09.25, (b) 2021.10.10, (c) 2021.11.15, (d) 2021.12.09, (e) 2022.01.11, (f) 2022.02.25, and (g) 2022.03.09.

boundaries. The main reason is the high volume of shipping channels and busy cargo transportation in these areas, which leads to lower sea surface chlorophyll concentrations. From March to September each year, owing to the discharge of domestic sewage and other pollutants, the nearshore areas have high levels of nutrients and the water temperature is suitable, leading to the rapid reproduction of marine life and an increase in sea surface chlorophyll concentration.

## 5. Conclusion and Prospects

This study is oriented towards the CZI remote sensing data obtained by China's ocean color satellite HY-1C. We developed a remote sensing reversion model for sea surface chlorophyll concentration, which is suitable for China's coastal waters, and achieved the remote sensing reversion of sea surface chlorophyll concentration in the Zhoushan Archipelago and its coastal waters.

- (1) Band sensitivity analysis was performed. For the CZI remote sensing data obtained using China's ocean color satellite HY-1C, the bands with the highest correlation to sea surface chlorophyll concentration are  $B3/B2$  and  $B3/(B2 + B1)$ , with correlation coefficients both being 0.77.

- (2) A remote sensing inversion model for sea surface chlorophyll concentration was constructed on the basis of CZI remote sensing data from China's ocean color satellite HY-1C. The quadratic polynomial model ( $y = 105.42x^2 - 175.67x + 75.167$ ), using  $B3/B2$  as the independent variable, had the highest  $R$ -square at 0.9107. The average error between the field-measured data and the model results was 26.85%.
- (3) The remote sensing reversion of sea surface chlorophyll concentration in the Zhoushan Archipelago and its coastal waters has been achieved. The spatial distribution characteristics of sea surface chlorophyll concentration are evident, with higher concentrations in the coastal waters where human activities are more intensive and lower concentrations in the coastal waters farther from land.

There are some shortcomings in this study. First, the sampling sites were concentrated in a limited area around the island, which leads to the limitation of the constructed model. Therefore, more field-measured data from coastal waters will be added to optimize the model and improve its accuracy in the future. Second, the coastal zone is cloudy and rainy, which restricts the application of a single image. Therefore, producing monthly sea surface chlorophyll concentration products based on multi-temporal HY-1C CZI remote sensing data is another research topic in the future.

### Acknowledgments

This work was supported by the National Natural Science Foundation of China (Grant No. 42171311) and the Open Fund of State Key Laboratory of Remote Sensing Science (Grant No. OFSLRSS202218).

### Declaration of Competing Interest

The authors declare that they have no known competing financial interests or personal relationships that could have appeared to affect the work reported in this paper.

### References

- 1 W. J. Moses, A. A. Gitelson, S. Berdnikov, and V. Povazhnyy: Environ. Res. Lett. **4** (2009) 045005. <https://doi.org/10.1088/1748-9326/4/4/045005>
- 2 F. Zhai, Z. Liu, Y. Gu, S. He, Q. Hao, and P. Li: J. Geophys. Res.: Oceans **128** (2023) e2022JC019528. <https://doi.org/10.1029/2022JC019528>
- 3 S. Hafeez, M. S. Wong, H. C. Ho, M. Nazeer, J. Nichol, S. Abbas, D. Tang, K. H. Lee, and L. Pun: Remote Sens. **11** (2019) 617. <https://doi.org/10.3390/rs11060617>
- 4 K. Zhang, X. Zhao, J. Xue, D. Mo, D. Zhang, Z. Xiao, W. Yang, Y. Wu, and Y. Chen: Front. Mar. Sci. **10** (2023) 1212992. <https://doi.org/10.3389/fmars.2023.1212992>
- 5 N. Pahlevan, B. Smith, J. Schalles, C. Binding, Z. Cao, R. Ma, K. Alikas, K. Kangro, D. Gurlin, N. Hà, B. Matsushita, W. Moses, S. Greb, M. K. Lehmann, M. Ondrusek, N. Oppelt, and R. Stumpf: Remote Sens. Environ. **240** (2020) 111604. <https://doi.org/10.1016/j.rse.2019.111604>
- 6 C. Hu, Z. Lee, and B. Franz: J. Geophys. Res.: Oceans **117** (2012) C1011. <https://doi.org/10.1029/2011JC007395>
- 7 T. J. Browning and C. M. Moore: Nat. Commun. **14** (2023) 5014. <https://doi.org/10.1038/s41467-023-40774-0>
- 8 G. A. J. Sandamali, E. P. D. N. Thilakarathne, W. N. D. S. Jayarathna, A. P. Abeygunawardana, T. W. S. Warnasuriya, and K. P. U. T. Egodauyana: Reg. Stud. Mar. Sci. **61** (2023) 102904. <https://doi.org/10.1016/j.rsma.2023.102904>

- 9 M. N. Hidayat, R. Wafdan, M. Ramli, Z. A. Muchlisin, and S. Rizal: *Global J. Environ. Sci. Manage.* **9** (2023) 389. <https://doi.org/10.22034/gjesm.2023.03.03>
- 10 G. K. Das: *Knowledge-Based Eng. Sci.* **5** (2024) 19. <https://doi.org/10.51526/kbes.2024.5.2.19-30>
- 11 M. Nazeer and J. E. Nichol: *J. Hydrol.* **532** (2016) 80. <https://doi.org/10.1016/j.jhydrol.2015.11.037>
- 12 G. Zheng and P. M. DiGiacomo: *Remote Sens. Environ.* **201** (2017) 331. <https://doi.org/10.1016/j.rse.2017.09.008>
- 13 C. Neil, E. Spyarakos, P. D. Hunter, and A. N. Tyler: *Remote Sens. Environ.* **229** (2019) 159. <https://doi.org/10.1016/j.rse.2019.04.027>
- 14 W. Luo, R. Li, F. Shen, and J. Liu: *Remote Sens.* **15** (2023) 386. <https://doi.org/10.3390/rs15020386>
- 15 P. V. Zimba and A. Gitelson: *Aquaculture* **256** (2006) 272. <https://doi.org/10.1016/j.aquaculture.2006.02.038>
- 16 D. Xuan, Q. Hu, Y. Wang, H. Yang, L. Li, and L. Wang: *Water* **12** (2020) 829. <https://doi.org/10.3390/w12030829>
- 17 Z. Wei, X. Jiao, Y. Du, J. Zhang, H. Pan, G. Wang, D. Wang, and Y. P. Wang: *Ocean Coastal Manage.* **237** (2023) 106516. <https://doi.org/10.1016/j.ocecoaman.2023.106516>
- 18 C. Chen, H. Chen, J. Liang, W. Huang, W. Xu, B. Li, and J. Wang: *Remote Sens.* **14** (2022) 3001. <https://doi.org/10.3390/rs14133001>
- 19 J. Aristegui, P. Tett, A. Hernández-Guerra, G. Basterretxea, M. F. Montero, K. Wild, P. Sangrá, S. Hernández-Leon, M. Canton, J. A. García-Braun, M. Pacheco, and E. D. Barton: *Deep Sea Res. Part I* **44** (1997) 71. [https://doi.org/10.1016/S0967-0637\(96\)00093-3](https://doi.org/10.1016/S0967-0637(96)00093-3)
- 20 E. Spyarakos, L. G. Vilas, J. M. T. Palenzuela, and E. D. Barton: *Remote Sens. Environ.* **115** (2011) 2471. <https://doi.org/10.1016/j.rse.2011.05.008>
- 21 H. Ji, L. Tian, J. Li, R. Tong, Y. Guo, and Q. Zeng: *IEEE J. Sel. Top. Appl. Earth Obs. Remote Sens.* **14** (2020) 1693. <https://doi.org/10.1109/JSTARS.2020.3045516>
- 22 J. Jiao, Y. Lu, and C. Hu: *Remote Sens. Environ.* **308** (2024) 114205. <https://doi.org/10.1016/j.rse.2024.114205>
- 23 J. Liu, X. Ye, Q. Song, J. Ding, and B. Zou: *National Remote Sensing Bulletin* **27** (2023) 1. <https://doi.org/10.11834/jrs.20235002>
- 24 X. Zhao, Y. Ma, Y. Xiao, J. Liu, J. Ding, X. Ye, and R. Liu: *ISPRS J. Photogramm. Remote Sens.* **205** (2023) 147. <https://doi.org/10.1016/j.isprsjprs.2023.10.006>
- 25 C. Hu, L. Feng, Z. Lee, B. A. Franz, S. W. Bailey, P. J. Werdell, and C. W. Proctor: *J. Geophys. Res.: Oceans* **124** (2019) 1524. <https://doi.org/10.1029/2019JC014941>
- 26 J. Kravitz, M. Matthews, S. Bernard, and D. Griffith: *Remote Sens. Environ.* **237** (2020) 111562. <https://doi.org/10.1016/j.rse.2019.111562>
- 27 M. Shin, Y. Kang, S. Park, J. Im, C. Yoo, and L. J. Quackenbush: *GISci. Remote Sens.* **57** (2020) 174. <https://doi.org/10.1080/15481603.2019.1703288>
- 28 G. Kim, S. Lee, J. Im, C. Song, J. Kim, and M. Lee: *GISci. Remote Sens.* **58** (2021) 1175. <https://doi.org/10.1080/15481603.2021.1972714>
- 29 A. De Myttenaere, B. Golden, B. Le Grand, and F. Rossi: *Neurocomputing* **192** (2016) 38. <https://doi.org/10.1016/j.neucom.2015.12.114>
- 30 S. Kim and K. Heeyoung: *Int. J. Forecasting* **32** (2016) 669. <https://doi.org/10.1016/j.ijforecast.2015.12.003>